Investigation of in vitro anticancer and DNA strap interactions in live cells using carboplatin type Cu(II) and Zn(II) metalloinsertors

ARTICLE *in* EUROPEAN JOURNAL OF MEDICINAL CHEMISTRY · AUGUST 2014

Impact Factor: 3.45 · DOI: 10.1016/j.ejmech.2014.08.036 · Source: PubMed

2 AUTHORS:

Narayanaperumal Pravin
Virudhunagar Hindu Nadars' Senthikumara…
15 PUBLICATIONS **39** CITATIONS
SEE PROFILE

Raman Natarajan
Virudhunagar Hindu Nadars' Senthikumara…
158 PUBLICATIONS **1,674** CITATIONS
SEE PROFILE

European Journal of Medicinal Chemistry 85 (2014) 675–687

Contents lists available at ScienceDirect

European Journal of Medicinal Chemistry

journal homepage: http://www.elsevier.com/locate/ejmech

Original article

Investigation of *in vitro* anticancer and DNA strap interactions in live cells using carboplatin type Cu(II) and Zn(II) metalloinsertors

Narayanaperumal Pravin, Natarajan Raman*

Research Department of Chemistry, VHNSN College, Virudhunagar 626 001, India

ARTICLE INFO

Article history:
Received 28 June 2014
Received in revised form
8 August 2014
Accepted 9 August 2014
Available online 12 August 2014

Keywords:
Cu(II) and Zn(II) metalloinsertors
Carboplatin
Cyclobutane-1,1-dicarboxylic acid
Reactive oxygen species
Antitumor activity

ABSTRACT

A series of carboplatin type Cu(II) and Zn(II) metalloinsertors (**1**–**8**) having β-diketone analogues and biologically significant cyclobutane-1,1-dicarboxylic acid have been synthesized and characterized by spectral and analytical methods. The binding and cleavage propensity of these metalloinsertors on DNA and their cytotoxic effects in live cells have been explored. From the gel electrophoresis study, it is observed that the complexes **1**–**8** cleave pBR322 DNA *via* a hydrolytic mechanism induced by hydroxyl radical scavengers, DMSO and EtOH as the reactive oxygen species (ROS). *In vivo* antitumor efficacy has been studied on EAC tumor bearing mice which is assessed by mean survival time, effect on hematological parameters and solid tumor volume. The results strongly support that complex **1** shows potent antitumor effect against EAC and higher than the standard drug carboplatin. Moreover, the cytotoxicity of the complexes, screened on a panel of human cancerous cell lines *viz.*, human cervical cancer cells (HeLa), human breast adenocarcinoma cells (MCF-7), human laryngeal epithelial carcinoma cells (HEp-2), human liver carcinoma cells (Hep G2) and non-cancerous NIH 3T3 mouse embryonic fibroblasts cell lines, reveals that complex **1** exhibits a better anticancer activity than other complexes and standards.

1. Introduction

Over the past decades, metallopharmaceuticals are known to act on DNA by inhibiting DNA replication and transcription. Thus, studies on the interaction of metal complexes with DNA may reveal useful information on the rational drug design and development of perceptive chemical probe for DNA [1,2]. To date, cisplatin is considered to be one of the most successful and extensively used as anticancer drugs. Second generation platinum drugs including cisplatin, oxaliplatin and carboplatin have been developed for clinical application [3]. Among them, carboplatin displays a more tolerable toxicological profile due to the higher stability of the chelating 1,1-cyclobutanedicarboxylato ligand when compared to the chlorido ligands in cisplatin. This in turn affects the administration of the drugs [4]. These limitations have aroused curiosity towards the design and evaluation of metal complexes other than platinum derivatives for therapeutic use. In this esteem, non platinum metal complexes predominantly low molecular weight metals such as copper and zinc are being used at the forefront of many of these efforts due to their stable, inert and low toxicity towards normal cells which are tremendously valuable in biological systems [5–9].

In recent times, dicarboxylic acids have been widely used as a polydentate ligand involving in diverse reactions to complexes which have interesting properties in biological systems. Many different bridging ligands such as pyridine (di)carboxylic acids and imidazole (di)carboxylic acids [10,11] have effectively been familiar with the construction of coordination compounds. These ligands have diversiform coordination modes, and they contain two carboxyl groups. This trait could increase the water-solubility of the compounds for the cell membrane and thus facilitate the entrance into the cell [12]. It is prominent that Schiff bases belong to a class of organic compounds which have potential biological profile, indeed the activity of these compounds augment when they complex with metal ions [13]. This factor defends the drug against enzymatic degradations because of the inertness of certain metal–ligand linkages which have better hydrophobicity/hydrophilicity properties than the free ligand and through this it can improve the transport process in the tissues. Moreover, the complexation can liberate the active drug(s) in a specific organ, and its action can be reinforced by the combination of effects from the ligands and from the metal residue. The application of these principles has previously resulted in the design of victorious metal based drugs [14,15]. Many studies suggest that DNA is the primary intracellular target of

* Corresponding author.
E-mail addresses: pravinknp2012@gmail.com (N. Pravin), drn_raman@yahoo.co.in, ramchem1964@gmail.com (N. Raman).

http://dx.doi.org/10.1016/j.ejmech.2014.08.036
0223-5234/

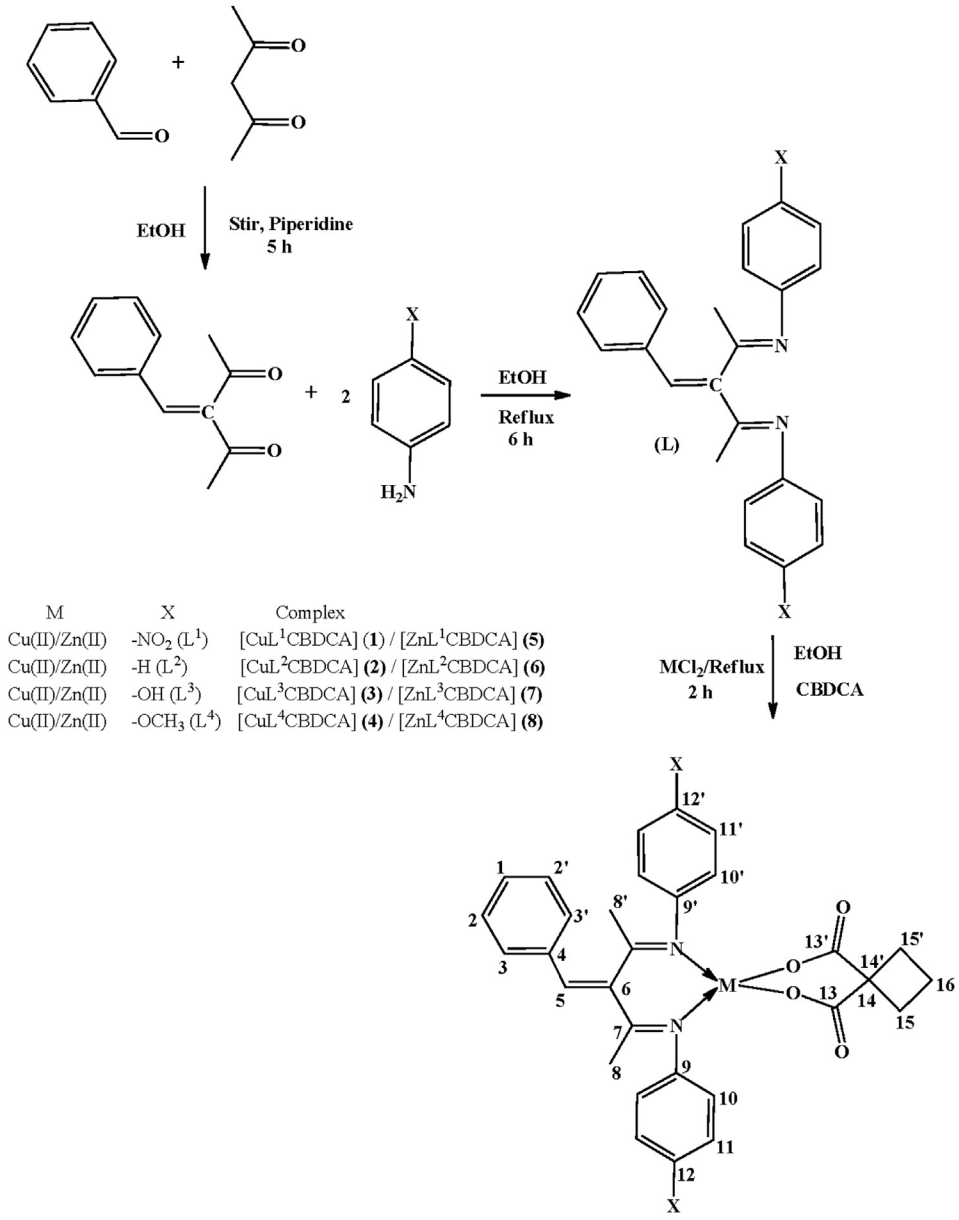

Scheme 1. Synthesis of Schiff base ligands and their metal complexes.

antitumor drugs because the interaction between small molecules and DNA can cause DNA damage in cancer cells [16–18]. Thus, to facilitate the development of new potential DNA targeting antitumor drugs, the binding mechanisms of metal complexes to DNA should be premeditated.

Our group has continuously been interesting in DNA interactions of mixed-ligand complexes and has reported the synthesis, DNA binding and cleavage activity of various transition metal complexes [19,20]. In continuation of our journey in designing and exploring the newer anticancer agents [21,22] in order to improve the anticancer efficacy, we hereby report the synthesis and characterization of few novel carboplatin type Cu(II) and Zn(II) complexes. Furthermore, the *in vitro*, *in vivo* (EAC tumor model) and DNA strap interactions and antitumor activities against four human cancer cell lines along with one normal mouse embryonic fibroblasts cell line have been probed.

2. Chemistry

The analytical, physicochemical and electronic spectral parameters of mixed ligand (*i.e.*, cyclobutane-1,1-dicarboxylic acid) complexes are compiled in the experimental section. The complexes are found to be air stable. The ligands are soluble in common organic solvents but their complexes are soluble only in DMF and DMSO. The results of elemental analysis for the metal complexes are in good agreement with the calculated values showing that the complexes have 1:1:1 (Knoevenagel condensate Schiff base: metal: cyclobutane-1,1-dicarboxylic acid) stoichiometry of the type [ML(CBDCA)] wherein L acts as a bidentate ligand. The metal(II) complexes are dissolved in DMF and the molar conductivities of 10^{-3} M of their solution at room temperature are measured. The lower conductance values (9.6–16.3 Ω^{-1} cm^2 mol^{-1}) of the complexes support their non-electrolytic nature.

3. Pharmacology

The DNA strap interaction of the synthesized complexes with CT DNA was carried out by electronic absorption spectroscopy, viscosity measurements, cyclic voltammetry and differential pulse voltammetry techniques. The extent of pBR322 DNA damage, in the absence and presence of an activators *viz.*, H_2O_2, AH_2, MPA and GSH and various radical scavengers like sodium azide NaN_3 (singlet oxygen), SOD (superoxide), DMSO, EtOH (hydroxyl radical scavenger) was monitored using agarose gel electrophoresis. A scrupulous sympathetic of the structural and electronic properties of drug-DNA complexes and their mechanism of binding is the key step in elucidating the principles of their anti-cancer activity. *In vitro* and *in vivo* anti-tumor functions of synthesized complexes against Ehrlich ascites carcinoma (EAC) tumor model were investigated. The antitumor activity was assessed by hematological parameters, median survival time and cell viability with trypan blue dye exclusion assay. *In vitro* cytotoxicity was performed by MTT assay against human cervical cancer cell lines (HeLa), human breast cancer (MCF-7), human laryngeal epithelial carcinoma (HEp-2) cells, human liver carcinoma (Hep G2) and normal NIH 3T3 (mouse embryonic fibroblasts). The minimum inhibitory concentration (MIC) values of the complexes were determined.

4. Results and discussion

The synthetic pathways of the formation of Schiff bases and their mixed ligand complexes are sketched in Scheme 1. The ligands and their complexes are found to be stable in air. The ligands are soluble in common organic solvents but their complexes are soluble only in DMF and DMSO.

4.1. Infrared spectra

In IR spectra, the ν(C═N) band presented in the ligands is shifted to lower frequency by *ca.*30 cm^{-1}on complexation [23]. The free −OH group of the ligand L^3 vibrated at *ca.* 3435 cm^{-1} does not show any significant shift on complex formation. The additional bands observed in complexes at 1683, 1349 and 817 cm^{-1} are ascribed to the vibrations of the carboxylate moiety. Therefore, the cyclobutane-1,1-dicarboxylic acid acts as bidentate coordinated to the metal(II) centers *via* two monodentate carboxylate groups. The mixed ligand complexes show the stretching vibration of ν(C═O) of the cyclobutanedicarboxylato groups at 1677–1689 cm^{-1}. The relatively high value for this group shows the unsharing of the C═O group in coordination to metal ion and thus the cyclobutanedicarboxylato group acts as a dianionic bidentate ligand. This is further confirmed by the formation of metal–oxygen bond in the complexes in the region 511–529 cm^{-1}. The new band observed in the complexes in the range 430–448 cm^{-1} indicates the formation of metal–nitrogen bond.

4.2. Elemental analysis and molar conductivity measurements

The results of elemental analysis for the metal complexes are in good agreement with the calculated values showing that the complexes have 1:1:1 metal–ligand stoichiometry of the type [ML(CBDCA)] wherein both L and CBDCA act as bidentate ligands (L = Knoevenagel condensed Schiff bases; CBDCA = cyclobutane-1,1-dicarboxylic acid) (Scheme 1). The complexes are found to be non-electrolytic nature in 10^{-3} M DMF solution, implying the replacement of chloride anions by bidentate carboxylato group to the central metal ion. The absence of counter (chloride) ions is conformed from Volhard's test. The molar conductance values (9.6–16.3 Ω^{-1} cm^2 mol^{-1}) of the complexes support their non-electrolytic nature [24].

4.3. Magnetic moments and electronic spectra

The geometry of the metal complexes has been deduced from electronic spectra and magnetic data of the complexes which are recorded in DMF solution. The free ligands exhibit two intense bands in 45,857–41,656 and 28,361–27,138 cm^{-1} region due to $\pi \rightarrow \pi^*$ and $n \rightarrow \pi^*$ transitions [25], respectively. In all the metal complexes, the absorption bands at 43,759–41,424 and 29,302–27,659 cm^{-1} are due to $\pi \rightarrow \pi^*$ and $n \rightarrow \pi^*$ transitions that are observed in the spectra of the free ligands L^1, L^2, L^3 and L^4. These transitions are shifted to blue or red frequencies due to the coordination of the ligand with metal ions. The electronic spectra of Cu(II) complexes **1**–**4** reveal a broad band in the region 21,786–21,413 cm^{-1} with high molar intensities (ε = 1058–1113 L M^{-1} cm^{-1}) assigned to $^2B_{1g} \rightarrow {}^2A_{1g}$ transition suggesting distorted square planar environment around the Cu(II) ion. The observed magnetic moment of the Cu(II) complexes **1**–**4** (1.85–1.89 B.M) at room temperature indicates the non-coupled mononuclear complexes of magnetically diluted d^9 system with S = 1/2 spin-state. The monomeric nature of the complexes is further supported by the microanalytical and ESI mass spectral data. The electronic absorption spectra of the diamagnetic Zn(II) complexes show the bands in the region 40,762–42,451 and 29,395–33,169 cm^{-1} which are assigned to intra-ligand charge transfer transitions [26].

4.4. NMR spectra of zinc complexes

In ^{1}H NMR, a set of multiplets appeared in the range of 6.8–7.4 δ for all the ligands and their Zn(II) complexes are assigned to the aromatic region. The phenolic −OH proton for L^3 ligand and its zinc complex is observed as a singlet at *ca.* 10.3 ppm. It is suggesting that phenolic −OH group is not taking part in the complexation. ^{1}H NMR spectra of aliphatic methyl protons exhibit peaks at 2.1–2.3 ppm for all the Schiff base ligands and their Zn(II) complexes. There is no appreciable change in all other signals of the complexes **5**–**8**.

The ^{13}C NMR spectra of the ligands show aromatic carbons at 119–129 ppm. The ligands also show the C═N carbons at 172.8–175.4 ppm, which are shifted to downfield at 170.1–170.6 δ, upon coordination indicating the participation of C═N groups in complex formation. ^{13}C NMR spectra of ligand L^4 and its Zn(II) complex **8** are given in Fig. S1. The appearance of signals for the group COO^- at 61.2 and 164.3–168.7 δ indicates the presence of CBDCA carbon moiety. Further, in all the zinc complexes (**5**–**8**) the particular signals of CBDCA carbon moiety have been appeared at the regions 175.9, 25.7, 136.7 and 129.6 ppm. This indicates the coordination of the ligand to the metal ion.

4.5. Mass spectra

The ESI-mass spectra of synthesized ligands and their complexes have been recorded and the obtained molecular ion peaks authenticate the proposed formulae. The mass spectrum of L^1 ligand shows [M+1] peak at *m*/*z* 429 (86.4%) corresponding to $[C_{24}H_{20}N_4O_4]^+$ ion. Also, the spectrum exhibits the fragments at *m*/*z* 184 (35.2%), 102 (40.3%) and 77 (20.4%) corresponding to $[C_{12}H_{12}N_2]^+$, $[C_8H_6]^+$ and $[C_6H_5]^+$ respectively. ESI mass spectra of ligand L^1 and its Cu(II) complex **1** are shown in Fig. S2. The mass spectrum of [CuL^1(CBDCA)] shows peaks at *m*/*z* 635 with 54.5% abundance. The strongest peak (base beak) at *m*/*z* 429 (66.8%) represents the stable species $C_{24}H_{20}N_4O_4$. Moreover, the spectrum exhibits the fragments at *m*/*z* 184, 102 and 77 corresponding to

$[C_{12}H_{12}N_2]^+$, $[C_8H_6]^+$ and $[C_6H_5]^+$ respectively. The *m*/*z* of all the fragments of ligands and their complexes confirm the stoichiometry of the complexes as $[CuL^1(CBDCA)]$. The observed peaks are in good agreement with their formulae as expressed from microanalytical data. Thus, the mass spectral data reinforce the conclusion drawn from the analytical and conductance values.

4.6. EPR spectra

The X-band EPR spectra of all Cu(II) complexes (**1**–**4**) have been recorded in DMSO at liquid nitrogen temperature and at room temperature. The EPR spectra of Cu(II) complexes **1** and **4** both at room temperature (273 K) and liquid nitrogen temperature (77 K) are depicted in Fig. 1. The spectrum of the copper complex **1** at RT shows one intense absorption band in the high field and is isotropic due to the tumbling motion of the molecules. However, this complex at LNT shows three-well resolved peaks with low field region. The spin Hamiltonian parameters of the complexes have been calculated and are summarized in Table 1. From this spectral data, it is found that $A_{||}$ (131–138) > $A_{\perp}$ (24–29); $g_{||}$ (2.16–2.21) > $g_{\perp}$(2.03–2.05) > g_e(2.0023), which support the d^2_{x-y} as the ground state, characteristic of square planar geometry and axially symmetric. Further, in an axial symmetry, the g-values are related by the expression, $G = (g_{||}-2)/(g_{\perp}-2)$, which measures the exchange interaction between the copper centers in polycrystalline solid. The G values lie within the range 4.2–5.3 for all the copper complexes indicating negligible exchange interaction of Cu–Cu in the complexes according to Hathaway [27].

In order to quantify the degree of distortion of the Cu(II) complexes, the f factor ($g_{||}/A_{||}$) is obtained from the EPR spectra, where the f factor is regarded as an empirical index of tetrahedral distortion. Its value ranges between 105 and 135 for square planar complexes, depending on the nature of the coordinated atoms. Values of this factor may vary from 157 to 166 for extreme distortions in square planar complexes and it depends on the nature of the coordinated atoms. The f values of Cu(II) complexes are indicating significant distortion from planarity. In addition, the molecular orbital coefficients α^2 (covalent in-plane σ-bonding) and β^2 (covalent in-plane π-bonding) have been calculated from the following equations [28]:

$$\alpha^2 = \left(A_{||}/0.036\right) + \left(g_{||} - 2.0027\right) + \left(3/7\right)\left(g_{\perp} - 2.0027\right) + 0.04$$

$$\beta^2 = \left(g_{||} - 2.0027\right)E_{d-d}/\left(-8\lambda\alpha^2\right)$$

The calculated values of α^2 (0.69–0.77) and β^2 (0.87–0.96) for the complexes **1**–**4** indicate that the in plane σ-bonding and in-plane π-bonding are appreciably covalent and are consistent with very strong in-plane π-bonding in this complex. Furthermore, the nature of bonding in the Cu(II) complexes can be obtained from the

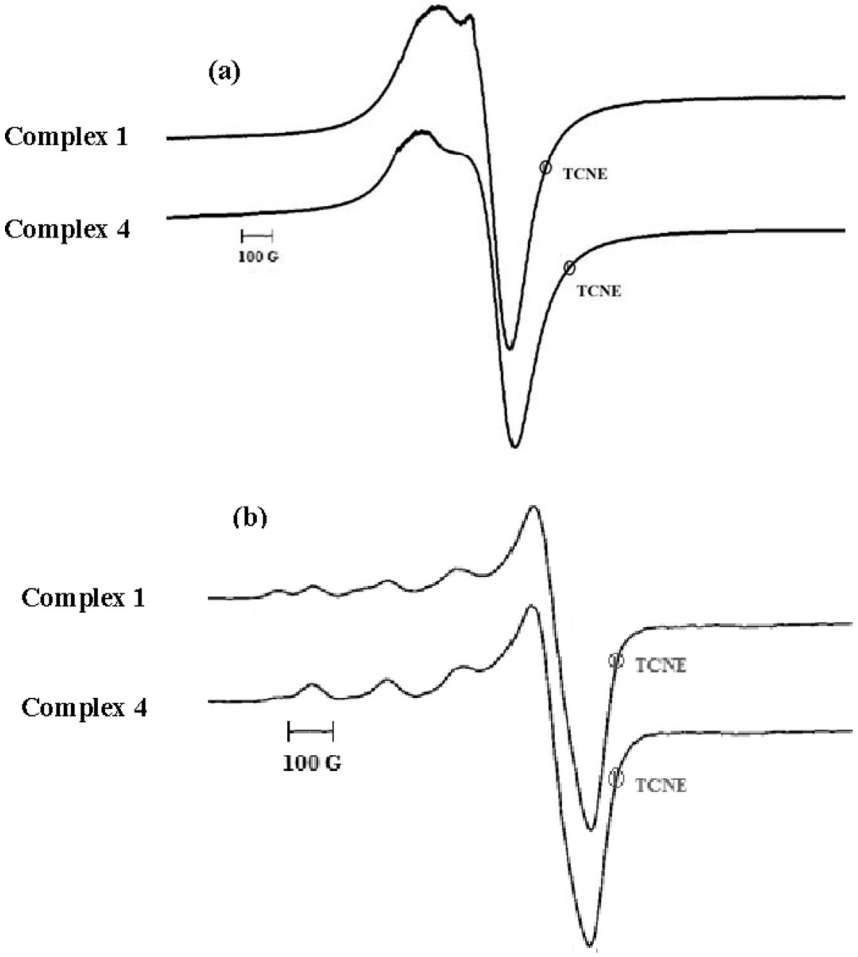

Fig. 1. X-Band EPR spectra of Cu(II) complexes **1** and **4** at room temperature (a) (273 K) and at liquid nitrogen temperature (b) (77 K).

Table 1
The spin Hamiltonian parameters of the Cu(II) complexes in DMSO solution at 77 K.

Complexes	g-tensor			$A \times 10^{-4}$ (cm^{-1})			f	G	α^2	β^2	$K_{\|}$	$K_{\perp}$
	$g_{\|}$	$g_{\perp}$	g_{iso}	$A_{\|}$	$A_{\perp}$	A_{iso}						
1	2.17	2.04	2.11	138	24	62	157	4.25	0.72	0.92	0.61	0.83
2	2.16	2.03	2.07	134	28	63	161	5.33	0.69	0.96	0.63	0.81
3	2.18	2.04	2.09	131	26	61	166	4.51	0.77	0.87	0.59	0.89
4	2.21	2.05	2.10	136	29	65	163	4.23	0.74	0.93	0.64	0.85

magnitude of the orbital reduction factors like $K_{||}$ and $K_{\perp}$ by using the following equations [29]:

$$K_{\|}^2 = \left(g_{\|} - 2.0027\right)E_{d-d}/8\lambda$$

$$K_{\perp}^2 = \left(g_{\perp} - 2.0027\right)E_{d-d}/2\lambda$$

In the present study of the above mentioned complexes, it is observed that $K_{||}$ (0.59–0.64) < $K_{\perp}$ (0.81–0.89) which indicates the presence of significant in-plane bonding. Based on the above observations, a square planar geometry is proposed for the complexes. In the absence of crystallographic data, the orbital reduction and bonding parameters of the Cu(II) complexes have provided supportive evidence to the conclusion obtained on the basis of electronic and magnetic moment values.

4.7. DNA fastening efficacy

4.7.1. Absorption titration measurement

Transition metal complexes can bind to DNA through covalent or non-covalent interactions [30]. The study of non-covalent interactions of transition metal complexes with DNA is an area of extreme modern curiosity. Since DNA is an important cellular receptor, many compounds wield their anticancer effects through binding to DNA, thereby altering the replication of DNA and inhibiting the growth of the tumor cells, which is the foundation for designing new and more efficient anticancer drugs, where their effectiveness depends on the mode and affinity of the binding [31]. Therefore, the binding studies of metal complexes to DNA are considered to be highly imperative in the development of new anticancer drugs. It is well known that the electronic absorption spectroscopy is widely employed to determine the propensity for binding of the complexes to DNA (CT DNA). In general, hyperchromism and hypochromism are the spectral features of DNA concerning changes of its double helix structure; hyperchromism means the breakage of the secondary structure of DNA and hypochromism shows that binding of complex to DNA can be due to electrostatic effect or intercalation which may stabilize the DNA duplex. Moreover, the existence of a red-shift is the indicative of stabilization of DNA duplex [32].

We have registered the spectra of solutions of the complexes **1** and **8** in the absence and in the presence of increasing concentrations of CT DNA which are exemplified in Fig. 2(a) and (b). In the UV region of the spectra, all the Cu(II) complexes exhibit an intense absorption around 338.2–386.0 nm and zinc complexes show bands in the region 324.5–380.3 nm (due to n–π* transition). With increase in DNA to complex ratio, hypochromism and red shift are observed in the range 8.5–20.8%, and their red shifts in the region 1.7–5.0 nm. The extent of binding strength of complexes is quantitatively determined by measuring an intrinsic binding constants K_b (Table 2). The intrinsic binding constant values of these complexes (**1**–**8**) are compared to cisplatin (standard drug) and ethidium bromide (classical intercalator) which reveal that K_b values of **1**–**8** are greater in magnitude (1.2–3.8 × 10^6 M^{-1}) than

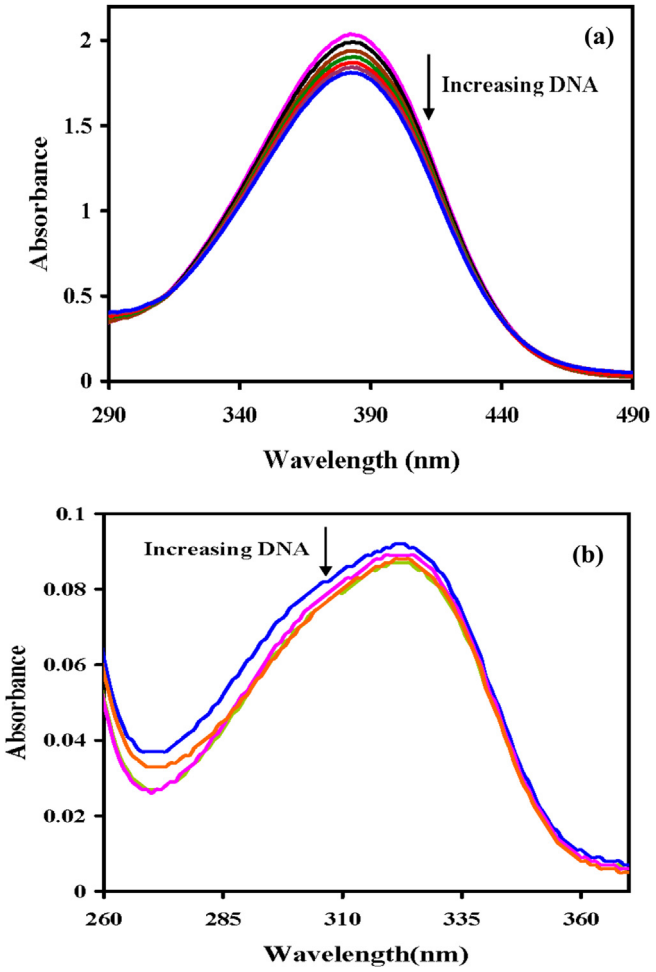

Fig. 2. Absorption spectra of complexes **1** (a) and **8** (b) in buffer pH = 7.2 at 25 °C in presence of increasing amount of DNA.

Table 2
Electronic absorption spectral properties of Cu(II) and Zn(II) mixed ligand complexes.

Complexes	λ_{max} (nm)		Δλ (nm)	[a]H%	[b]K_b (M^{-1})[c]
	Free	Bound			
1	386.0	381.0	5.0	20.8	3.8×10^6
2	342.5	339.3	3.2	8.5	2.6×10^5
3	340.6	337.8	2.8	10.7	1.3×10^6
4	338.2	336.5	1.7	14.5	1.6×10^6
5	380.3	376.5	3.8	18.2	2.7×10^6
6	351.4	348.1	3.3	9.2	2.1×10^5
7	353.3	350.2	3.1	11.2	1.2×10^6
8	324.5	320.5	4.0	12.3	1.5×10^6

[a] $H\% = [(A_{free} - A_{bound})/A_{free}] \times 100\%$.
[b] K_b = Intrinsic DNA binding constant determined from the UV–Vis absorption spectral titration.
[c] Error limit ±3%.

that of cisplatin ($5.73 \pm 0.45 \times 10^4$ M^{-1}) and ethidium bromide (1.4×10^6 M^{-1}) as reported in the literature [33,34] and relatively lower than the metallointercalator $[Ru(bpy)_2(HBT)]^{2+}$ (5.71×10^7 M^{-1}) [35]. However, the metal ions play a crucial role in DNA binding by these complexes. The binding strength of the synthesized complexes with DNA is shown as in the following order: **1** ≈ **5** > **2** ≈ **6** > **4** ≈ **8** > **3** ≈ **7**. The highest binding constant of complex **1** is due to electron withdrawing group present on the ligand moiety [36].

4.7.2. Hydrodynamic volume measurement

Though photophysical experiments afford necessary information about binding modes of metal complexes with DNA, but not provide conclusive evidences for the precise mode of binding. Hydrodynamic measurements are perceptive to DNA length change and considered to be the most decisive tests in assessing binding modes in solution in the absence of crystallographic structural data [37]. Classical intercalative mode causes a significant increase in viscosity of DNA solution due to separation of base pairs at intercalation sites and increase in overall DNA length. In contrast, complexes those bind exclusively in the DNA grooves typically cause less positive or negative or no change in DNA viscosity [38]. The viscosity of the DNA solution increases with increasing ratio of the complexes to DNA. As expected, the known DNA-intercalator, ethidium bromide (EB) increases the relative viscosity of DNA due to its strong intercalation. The effects of complexes together with the viscosity of rod-like DNA are shown in Fig. 3. Compared with EB, complexes demonstrate minor increase in the relative viscosity of CT DNA, suggesting an intercalation mode among the complexes and DNA. This result further suggests an intercalating binding mode of the complexes with DNA and also parallels the above photophysical results, such as hypochromism and red shift of the complexes in the presence of DNA. The experimental results suggest that complexes bind to DNA through a classical intercalation mode.

4.7.3. Electrochemical profiles

CV can afford useful information on the binding of metal complexes to DNA, because of the resemblance between the electrochemical and biological reactions. The application of the cyclic voltammetric technique to the study of interaction between the metal complexes and DNA provides a useful complement to the previously used spectral studies [39]. The cyclic voltammograms of the complexes **1** and **7** in the absence and presence of different amounts of DNA are shown in Fig. 4(a) and (b), exhibited significant shifts in the anodic and cathodic peak potentials followed by decrease in both peak currents, indicating the interaction existing among these complexes and CT DNA.

The voltammetric parameters obtained for all the complexes without and in the presence of DNA are given in Table 3. In the absence of CT DNA, the first redox cathodic peak appears at 0.048 V for Cu(II)→Cu(I) ($Ep_a = 0.066$ V, $Ep_c = 0.597$ V, $\Delta Ep = -0.114$ V and $E_{1/2} = -0.009$ V) and in the second redox couple, the cathodic peak appears at −0.103 V for Cu(I)→Cu(0) ($Ep_a = -0.416$ V, $Ep_c = -0.103$ V, $\Delta Ep = -0.358$ V, and $E_{1/2} = -0.282$ V). The Ip_a/Ip_c ratios for these two redox couples are 1.1 and 0.86 respectively. The voltammogram of the Zn(II) complex also shows quasi-reversible process. The reason for the quasi-reversible electron transfer process may be due to slow electron transfer or the adsorption of the complex onto the electrode surface [40]. A quasi-reversible transfer process with the redox couple [Zn(II)→Zn(0)] is observed for the complexes **5**–**8**. In complex **7**, the cathodic peak appeares at −0.172 V in the absence of DNA ($Ep_a = -0.867$ V, $Ep_c = -0.172$ V, $\Delta Ep = -0.695$ V, and $E_{1/2} = -0.520$ V). The Ip_a/Ip_c ratio is 1.08. This indicates the quasi-reversible redox process of the metal complexes. Incremental addition of DNA to the complex **7** results in a slight decrease in the current intensity and less negative shift of the oxidation peak potential. The resulting minor changes can be explained in terms of the slow diffusion of the complexes bound to the large DNA molecule.

In the differential pulse voltammogram of the complexes **1** and **7** obtained in the absence and the presence of varying amounts of DNA [in which a significant decrease in current intensity with

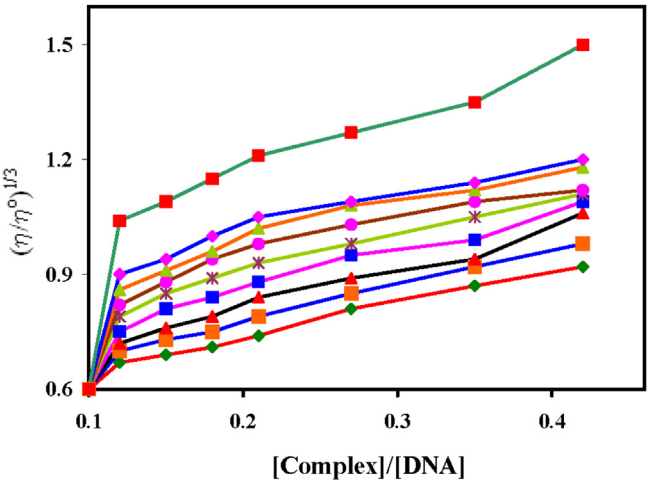

Fig. 3. Effect of increasing amount of [EB] (■), **1** (♦), **2** (▲), **3** (●), **4** (ж), **5** (■), **6** (▲), **7** (■) and **8** (♦) on the relative viscosity of DNA.1/R = [Complex]/[DNA] or [EB]/[DNA].

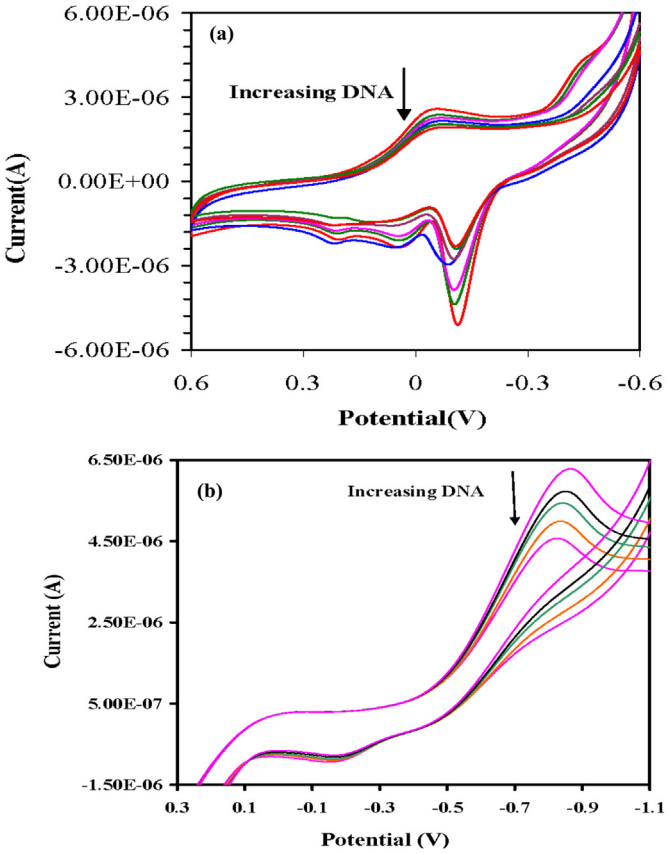

Fig. 4. Cyclic voltammograms of complexes **1** (a) and **7** (b) in buffer pH = 7.2 at 25 °C in presence of increasing amount of DNA.

Table 3
Redox potential profiles for interaction of DNA with Cu(II) and Zn(II) complexes.

Complexes	[a]ΔEp (V)		[b]$E_{1/2}$ (V)		I_{pa}/I_{pc}	$K_{[red]}/K_{[ox]}$
	Free	Bound	Free	Bound		
1	−0.204	−0.114	−0.013	−0.009	1.2	0.76
2	0.462	0.534	0.526	0.564	0.78	0.43
3	−0.128	−0.107	−0.186	−0.175	0.58	0.59
4	0.525	0.549	0.378	0.563	0.67	0.82
5	0.812	0.823	0.354	0.381	0.43	0.68
6	−0.119	0.248	−0.142	−0.128	3.21	0.79
7	−0.695	−0.677	−0.520	−0.492	1.08	0.54
8	0.167	0.178	−0.053	−0.045	0.84	0.93

Data from cyclic voltammetric measurements: [a]$\Delta Ep = Ep_a - Ep_c$; [b]$E_{1/2}$ is calculated as the average of anodic (Ep_a) and cathodic (Ep_c) peak potentials; [b]$E_{1/2} = Ep_a + Ep_c/2$.

increasing DNA concentration is observed (Fig. 5(a) and (b))], the shift in potential is related to the ratio of the binding constants by the following equation:

$$E_b - E_f = 0.0591 \log\left(K_{[red]} / K_{[ox]}\right)$$

where E_b and E_f are the peak potentials of the complex in its bound and free forms, respectively. In the present study, the novel mixed ligand complexes exhibit one-electron transfer during the redox process, and the Ip_c/Ip_a value is less than unity, indicating that the reaction of the complex on the glassy carbon electrode surface is quasi-reversible.

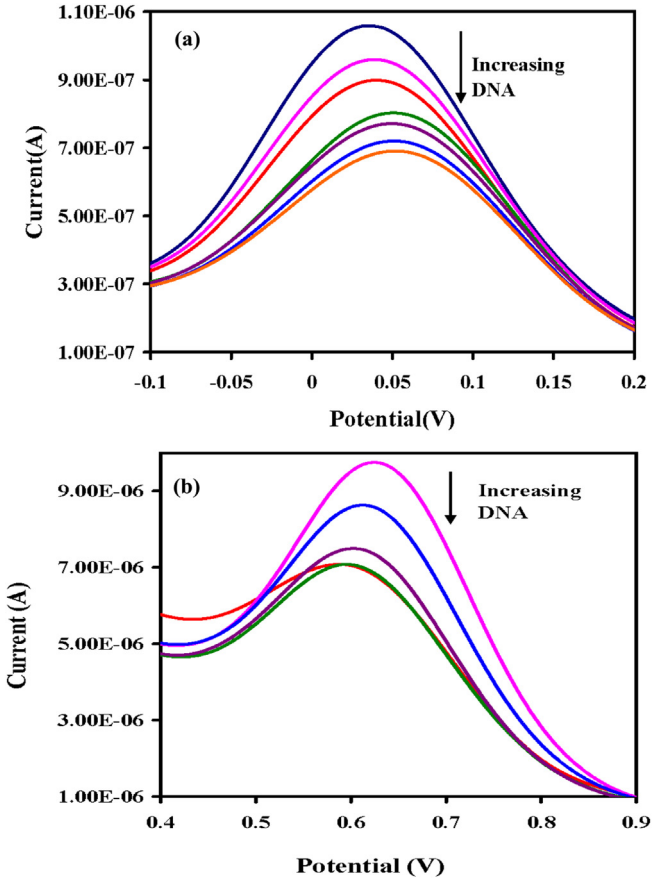

Fig. 5. Differential pulse voltammograms of **1** (a) and **7** (b) in buffer (pH = 7.2) at 25 °C in the presence of increasing amount of DNA. Arrow indicates the changes in voltammetric currents upon increasing the DNA concentration.

Table 4
Minimum inhibitory concentration of the synthesized compounds against growth of bacteria (μM).

Compound	Minimum inhibitory concentration (MIC) ($\times 10^4$ μM) SEM = ±2				
	Staphylococcus aureus	*Bacillus subtilis*	*Escherichia coli*	*Klebsiella pneumoniae*	*Salmonella typhi*
L^1	16.7	16.1	15.3	16.7	16.3
L^2	17.0	18.2	16.3	16.4	16.8
L^3	19.3	10.9	18.7	18.3	17.1
L^4	18.5	19.6	17.0	17.6	17.9
1	9.6	9.1	8.6	8.2	9.3
2	10.7	12.1	10.9	9.9	10.3
3	10.7	11.9	11.4	9.4	11.1
4	10.9	11.3	12.4	9.3	10.4
5	10.1	11.2	9.1	9.1	9.9
6	11.2	13.1	11.6	10.3	11.6
7	12.6	12.1	13.1	11.1	11.9
8	12.4	11.8	12.8	12.2	13.1
[a]Kanamycin	1.6	2.8	1.4	2.3	2.6

Average of 3 determinations, 3 replicates.
[a] Kanamycin is used as the standard.

4.8. Antimicrobial screening

As the antimicrobial screening contribution to the field of bioinorganic chemistry is important, the synthesized compounds have been evaluated for their antimicrobial actions. The results of the bactericidal and fungal study of the synthesized compounds are reported in Tables 4 and 5. Further, the antimicrobial action of ligands may be significantly enhanced on chelation with metal ions, but the activity is lesser than the standard drugs. Such enhanced activity of the complexes can also be explained on the basis of activation of enzymes, fineness of the particles, and size of the metal ion and the presence of substituted and highly conjugated β-diketimine analogous. The biological activity involves inhibition of DNA synthesis by creating lesions in DNA strands by oxidative rupture and by binding the nitrogen bases of DNA or RNA, hindering or blocking base replication. Due to the complexity of biological systems, it is rather difficult to stipulate the exact mechanism for such activities. However, the increased biocidal properties after complexation can be very well explained by Overtone's concept [41] and the Tweedy's Chelation theory [42]. The MIC values for the complexes are related to the nature of the *p*-substituent as they increase according to the following order *p*-(OCH_3 < OH < H < NO_2) [43]. This can be attributed to the fact that the effective nuclear charge experienced on d-electrons increases due to the presence of electron withdrawing *p*-substituents and decreases by the electron donating *p*-substituents.

4.9. DNA ripping actions

4.9.1. Interaction with pBR322 plasmid DNA

The potential of the cleavage DNA of the present complexes is studied by gel electrophoresis using supercoiled plasmid pBR322 DNA in TAE buffer (pH 7.4). When circular plasmid DNA is subjected to gel electrophoresis, relatively fast migration will be observed for the intact supercoil form (Form I). If scission occurs on one strand (nicking), the supercoil will relax to generate a slower moving open circular form (Form II). If both strands are cleaved, a linear form (Form III) that migrates between forms I and II will be generated. The cleavage of plasmid pBR322 DNA induced by Cu(II) and Zn(II) complexes is performed in the absence of external cofactor agents (either oxidant or reductant). The Cu(II) complexes are found to promote the cleavage of plasmid pBR322 DNA from the supercoiled form (I) to the nicked form (II) and linear form (III) (Fig. 6). No DNA cleavage has been observed for the control in which the metal

Table 5
Minimum inhibitory concentration of the synthesized compounds against the growth of fungi (μM).

Compound	Minimum inhibitory concentration (MIC) ($\times 10^4$ μM) SEM = ±2				
	Aspergillus niger	*Fusarium solani*	*Curvularia lunata*	*Rhizoctonia bataticola*	*Candida albicans*
L^1	16.2	17.4	15.5	14.9	16.4
L^2	18.9	18.5	17.6	15.8	17.6
L^3	20.3	21.6	19.5	17.5	18.4
L^4	19.2	19.0	18.1	16.9	17.9
1	9.4	10.3	10.9	12.2	14.6
2	11.3	11.7	13.0	14.1	15.5
3	12.1	15.2	11.3	15.2	16.1
4	12.6	15.0	13.6	14.3	17.1
5	12.9	12.1	14.4	15.5	16.4
6	15.4	14.3	18.2	17.1	18.1
7	18.1	14.0	16.3	17.6	16.5
8	13.1	15.3	15.5	16.9	18.9
[a]Fluconazole	1.4	1.7	1.2	1.5	1.8

[a] Fluconazole is used as the standard. Average of 3 determinations, 3 replicates.

complex is absent (lanes 2 and 3) and in presence of free $CuCl_2$ and $ZnCl_2$ (100 μM). When the concentrations of the Cu(II) and Zn(II) complexes are increased the amount of form I of pBR322 DNA diminishes gradually, whereas the amounts of form II and III increase. It shows, both the complexes are able to induce significant cleavage of the plasmid DNA even at the low concentration (5 μM). At the concentration of 30 μM, Cu(II) and Zn(II) complexes almost promote the complete conversion of DNA from form I to forms II and III (Fig. 6; lanes 4–11).

Moreover, the DNA cleavage activity of complexes **1** and **5** has been evaluated in the presence and absence of activators *viz.*; H_2O_2, AH_2, MPA and GSH as shown in Fig. 7. The results reveal that the cleavage activity of complexes are drastically enhanced in the presence of these activators and follows the order: MPA > H_2O_2 = GSH > AH_2 for complex **1** and MPA > GSH > AH_2 ≈ H_2O_2 for complex **5**. The complex **1** in the presence of activators exhibits momentous DNA cleavage activity, followed by complete degradation of DNA.

If the nuclease activity is quenched by the presence of any radical scavengers, it may be due to presence of reactive oxygen species (ROS). In order to investigate the role of reactive oxygen species which is responsible for the DNA cleavage mediated by complexes **1** and **5**, reactions are carried out in the presence of hydroxyl radical scavengers (DMSO and EtOH), singlet oxygen quencher (NaN_3) and superoxide oxygen scavenger (SOD) under identical conditions. As shown in Fig. 8, the addition of singlet oxygen scavenger (NaN_3) and superoxide scavenger (SOD) does not show any inhibitory effect (Fig. 8(a) lanes 8 and 9; Fig. 8(b) lanes 2 and 3) to the complexes **1** and **5**, while the addition of hydroxyl radical scavengers (EtOH and DMSO) shows significant inhibitory effects (Fig. 8(a) lanes 6 and 7; Fig. 8(b) lanes 4 and 5) and hence hydroxyl radical (OH•) is one of the ROS. Nevertheless, hydroxyl radical (OH•) is likely to be the reactive species responsible for the nuclease activity of plasmid DNA. From these observations, both the complexes **1** and **5** display efficient DNA cleavage activity through a hydrolytic cleavage induced by reactive oxygen species (ROS).

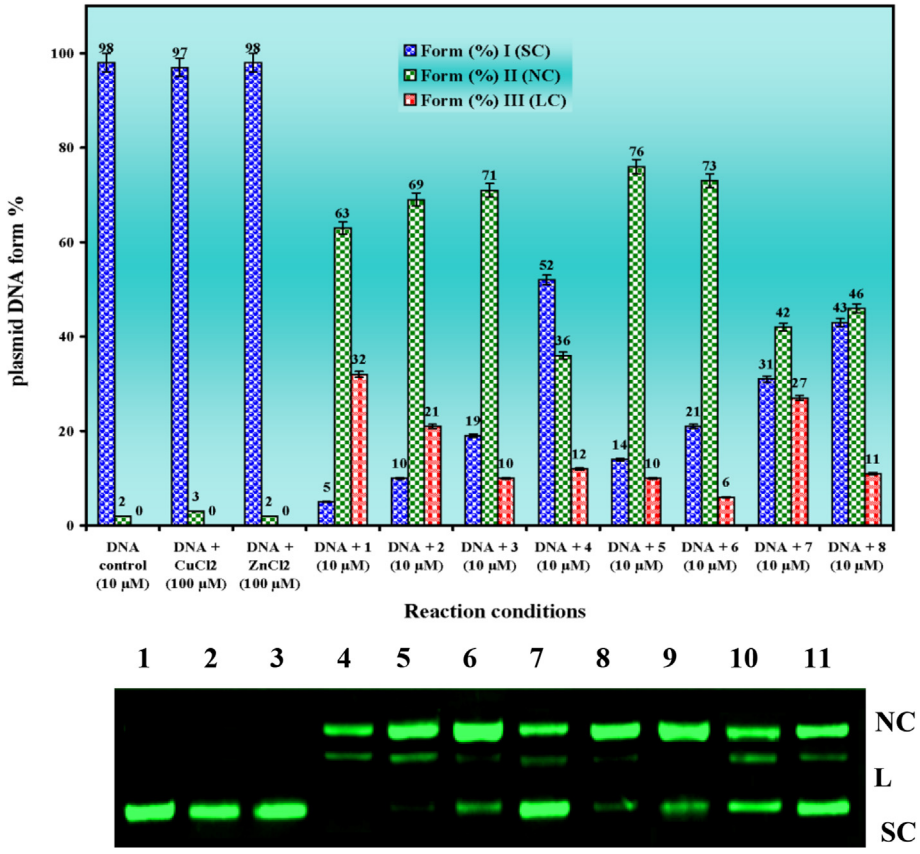

Fig. 6. Agarose gel electrophoresis pattern for the cleavage of pBR322 plasmid DNA (10 μM) by complexes **1**–**8** at 37 °C after incubation for 45 min at 30 μM concentration with histogram of % cleavage forms. lane 1: DNA control; lane 2: (100 μM) $CuCl_2$+ DNA; lane 3: (100 μM) $ZnCl_2$ + DNA; lane 4: complex **1** + DNA; lane 5: complex **2** + DNA; lane 6: complex **3** + DNA. lane 7: complex **4** + DNA; lane 8: complex **5** + DNA; lane 9: complex **6** + DNA; lane 10: complex **7** + DNA; lane 11: complex **8** + DNA.

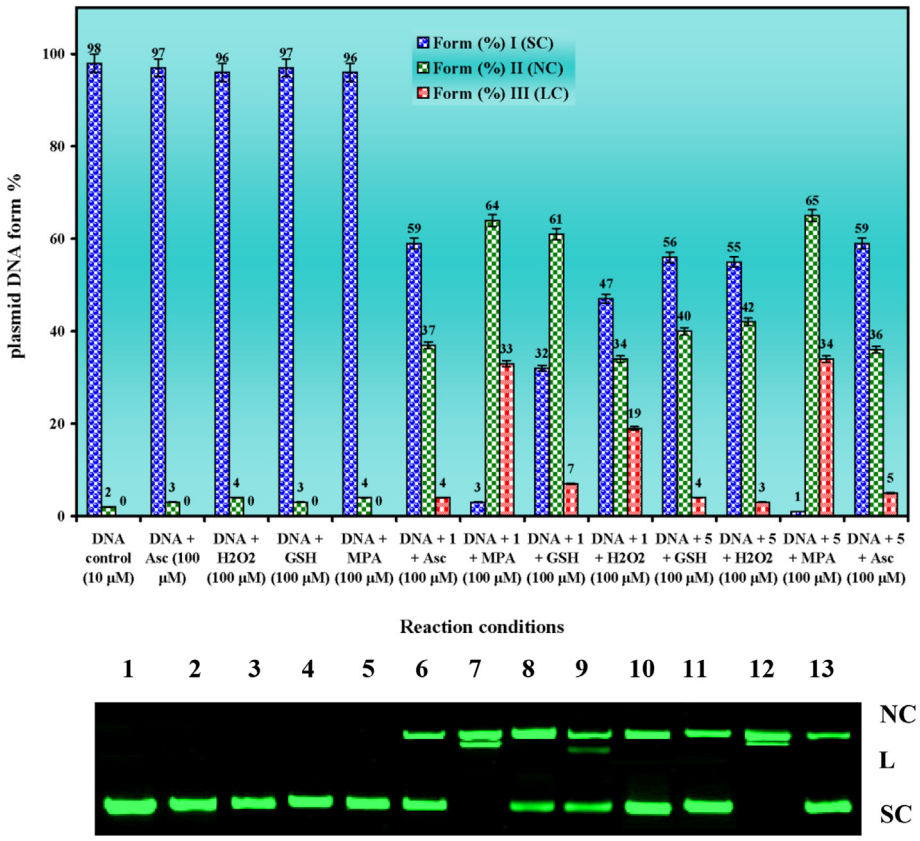

Fig. 7. Agarose gel electrophoresis pattern for the cleavage pattern of pBR322 DNA (10 μM) by complexes **1** and **5** at 37 °C after incubation for 45 min 30 μM concentration with histogram of % cleavage forms. In absence and presence of complex **1** with different activators: lane 1, DNA control; lane 2, DNA + Asc (100 μM); lane 3, DNA + H_2O_2 (100 μM); lane 4, DNA + GSH (100 μM); lane 5, DNA + MPA (100 μM); lane 6, DNA + **1** + Asc (100 μM); lane 7, DNA + **1** + MPA (100 μM); lane 8, DNA + **1** + GSH (100 μM); lane 9, DNA + **1** + H_2O_2 (100 μM); lane 10, DNA + **5** + GSH (100 μM); lane 11, DNA + **5** + H_2O_2 (100 μM); lane 12, DNA + **5** + MPA (100 μM); lane 13, DNA + **5** + AH_2 (100 μM).

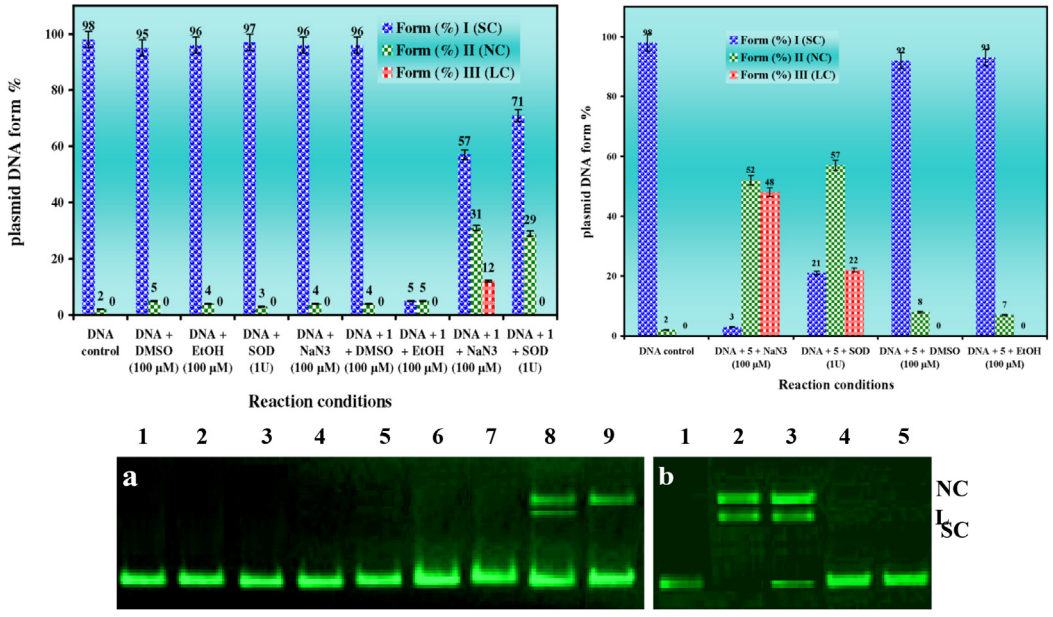

Fig. 8. Agarose gel electrophoresis pattern for the cleavage pattern of pBR322 DNA (10 μM) by complex **1** and **5** at 37C after incubation for 45 min 30 μM concentration with histogram of % cleavage forms. (a) In the absence and presence of complex **1** with different radical scavengers; lane 1, DNA control; lane 2, DNA + DMSO (100 μM); lane 3, DNA + EtOH (100 μM); lane 4, DNA + SOD (1U); lane 5, DNA + NaN_3 (100 μM); lane 6, DNA + **1** + DMSO (100 μM); lane 7, DNA + 1 + EtOH (100 μM); lane 8, DNA + **1** + NaN_3 (100 μM); lane 9, DNA + **1** + SOD (1U); (b) In the presence of complex **5** with different radical scavengers; lane 1, DNA control; lane 2, DNA + **5** + SOD (1U); lane 3, DNA + **5** + NaN_3 (100 μM); lane 4, DNA + **5** + DMSO (100 μM); lane 5, DNA + 5 + EtOH (100 μM).

Table 6
IC_{50} (μM) values of complexes, cisplatin and carboplatin against various cancer cell lines.

Compound	IC_{50} values (μM)				
	HeLa	HEp-2	Hep-G2	MCF-7	NIH 3T3
$CuCl_2$	524 ± 11	637 ± 17	465 ± 11	521 ± 13	176 ± 12
1	12.1 ± 1.6	11.8 ± 2.2	3.4 ± 0.21	13.8 ± 2.3	378 ± 4.2
2	14.2 ± 1.2	13.6 ± 1.8	4.8 ± 0.51	15.6 ± 1.9	346 ± 3.8
3	13.3 ± 1.5	12.7 ± 2.1	4.2 ± 0.40	14.8 ± 2.2	357 ± 4.5
4	12.8 ± 1.3	12.2 ± 2.6	3.8 ± 0.32	14.3 ± 2.7	366 ± 5.3
Cisplatin	12.6 ± 0.4	13.6 ± 0.9	12.1 ± 0.5	10.8 ± 1.6	198 ± 10
Carboplatin	12.3 ± 0.8	12.5 ± 1.2	6.9 ± 0.9	9.7 ± 1.3	243 ± 11

Average of 3 determinations, 3 replicates.
IC_{50}, Drug concentration inhibiting 50% cellular growth following 72 h of drug exposure.

4.10. In vitro cytotoxic profile

Cytotoxicity is a common limitation in stipulations of the introduction of new compounds into the pharmaceutical industry. The positive results obtained from the previous biological studies, namely, antimicrobial, DNA fastening and ripping studies for complexes **1**–**4**, encourage us to test their *in vitro* cytotoxic activity against a panel of human cancer cell lines along with normal mouse embryonic fibroblasts (NIH 3T3) cells by the MTT assay method. Cisplatin and carboplatin are used as positive controls to assess the cytotoxicity of the test compounds. The IC_{50} values show that the complexes **1**–**4** exhibit significant activity against HeLa, HEp-2, Hep-G2 and MCF-7 cell lines, which are almost equal to the activity of the well-known anticancer drugs, cisplatin and carboplatin (Table 6). Interestingly, on comparison of the IC_{50} value of the complexes **1**–**4** with cisplatin against Hep-G2, the inhibitory activity is about three times higher than that of cisplatin and two times than that of carboplatin (Fig. 9). These results also indicate that the IC_{50} value of the complexes **1**–**4** against NIH 3T3 (normal cells) is found to be lying in the range 346–378 μM, which confirms that the complexes are very specific for cancer cells and even less toxic compared to standard drugs (IC_{50} = 198 μM for cisplatin and 243 μM for carboplatin). It is clearly noted that the free $CuCl_2$ does not show any significant activity on all the cancer cells (IC_{50} = 465–642 μM), which confirms that the chelation of the ligand (nature of *p*-substituents) with the Cu(II) ion is the responsible factor for the observed varying cytotoxic properties of the complexes **1**–**4**. Also the better cytotoxic properties of the complexes may be attributed to the extended planar structure induced by the π–π* conjugation resulting from the chelation of the Cu(II) ion with the ligands. These findings confirm that the binding of the complex to DNA, which consequently leads to cell death.

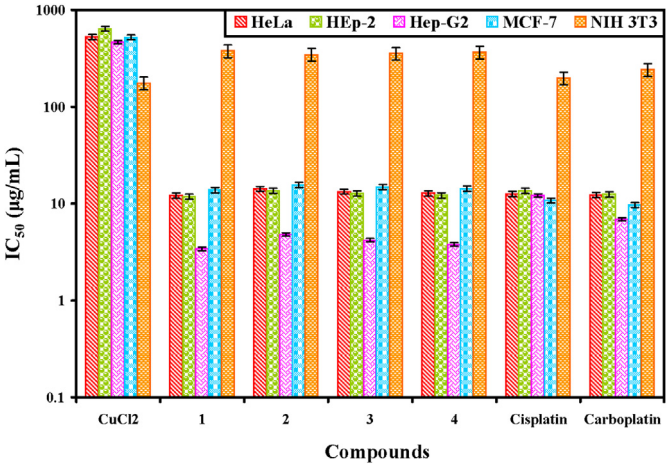

Fig. 9. The *in vitro* cytotoxicity of Cu(II) complexes against a panel of human cell lines.

4.11. In vivo effect on tumor screening

In vivo, there is a significant ($P < 0.001$) increase in mean survival time and increase in life span of the synthesized complexes **1**–**4** on EAC (41.34–31.21 and 135.75–112.87 at 100 mg kg^{-1}, respectively) in a dose dependent manner (Table 7). The results are almost comparable to that of cisplatin and carboplatin (40.66/44.28 and 151.60/162.37, respectively). In addition, the complexes **1**–**4** significantly ($P < 0.01$) reduce the tumor volume in dose dependent manner when compared to tumor control groups. The EAC tumor cells from ascitic fluid of different treatment groups are stained with Lieshman stain. They show marked cytological changes and cytolytic activity when compared to the respective tumor control cells (Fig. 10). The complexes **1**–**4** delay the cell division, thereby suggesting the reduction in EAC volume and increase survival time in mice. At the dose level 100 mg kg^{-1}, they are significantly improved the MST in tumor bearing mice. The prolongation of life span is a reliable criterion for judging efficacy of anticancer drugs [44,45] and the complexes **1**–**4** are able to meet this criterion. Myelosuppression and anemia (reduced hemoglobin) have been frequently observed in ascites carcinoma [46,47]. Anemia encounters in ascites carcinoma mainly due to iron deficiency, either by hemolytic or myelopathic conditions which finally lead to reduced RBC number [48]. In this study, elevated WBC count, reduces hemoglobin and RBC count are observed (Table 8) in EAC control mice and the oral administration of complex **1** restores hemoglobin content and maintains normal values of RBC and WBC, thus supporting its hematopoietic protecting activity without inducing myelotoxicity, the most common side effects of cancer chemotherapy. Therefore, further investigation in order to explore the potential of the complex **1** in tumor treatment may prove to be worthwhile.

5. Experimental protocols

The materials and methods for the newly synthesized mixed-ligand complexes are depicted as supplementary materials S1 (Supplementary Files). We acquired the probable composition of complexes as [ML(CBDCA)] (where M = Cu(II) and Zn(II); CBDCA = cyclobutane-1,1-dicarboxylic acid and L = Knoevenagel condensed Schiff bases) which were confirmed through elemental analyses, magnetic susceptibility, molar conductivity, NMR, UV, IR, EPR and mass spectra since no single crystals suitable for X-ray determination could be isolated.

Table 7
Effect of Cu(II) complexes treatment on the survival of tumor-bearing mice.

Treatment	MST	Increase in life span
Tumor control	16.26 ± 0.52	–
cis-platin	40.66 ± 0.81*	151.60
carboplatin	44.28 ± 0.81*	162.37
1	41.34 ± 0.27*	135.75
2	31.21 ± 0.57*	118.14
3	34.87 ± 0.71*	112.87
4	38.82 ± 0.34*	127.57

$N = 6$; d of drug treatment = 9, *$p < 0.01$ *versus* tumor control.
Data were analyzed by one-way ANOVA followed by Dunnett's test.

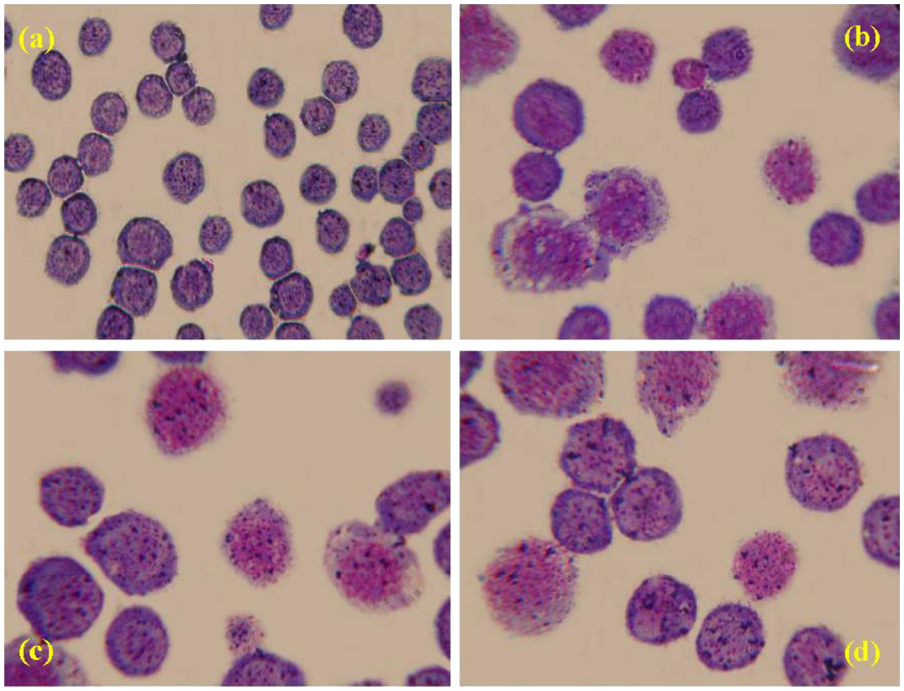

Fig. 10. (a) Smear showing matured EAC control cells (for 24 h) with definite cell wall and structure without degeneration, (b) EAC tumor cells treated with cisplatin for 24 h, (c) EAC tumor cells treated with carboplatin for 24 h and (d) complex **1** (for 24 h) treated with EAC cells showing degenerative changes like membrane blebbing, vacuolated cytoplasm and low staining intensity with complete destruction of cells.

The Schiff base ligands (L^1–L^4) were synthesized by the method reported in the literature by us [22]. To a stirred ethanolic solution of the above Schiff base(s) (5 mmol), a solution of copper(II)/zinc(II) chloride (0.67 g/0.68 g; 5 mmol) in ethanol was added dropwise. After the reaction for 1 h at 60 °C, a solution of cyclobutane-1,1-dicarboxylic acid (0.72 g; 5 mmol) in ethanol was added. The reaction solution was refluxed for 2 h. After cooling the reaction mixture to an ambient temperature, the formed solid was filtered, washed with diethyl ether and finally dried *in vacuum*.

[CuL^1(CBDCA)] (**1**) Yield: (1.9 g, 56%). m.pt: 182–187 °C. Anal. Calc. for $C_{30}H_{26}N_4O_8Cu$: Cu, 10.0; C, 57.0; H, 4.1; N, 8.8; Found: Cu, 9.9; C, 56.8; H, 3.9; N, 8.7 (%). IR (KBr pellet, cm^{-1}): 1686 ν(non-coordinated C=O in CBDCA); 1606 ν(−C=N); 1507 ν(−HC=C); 1473, 1312, 833 ν(−C–N str; $-NO_2$); 1329 ν(−C–O); 520 ν(M–O); 439 ν(M–N). MS *m/z*: 635 (54.5%) $[M+1]^+$. Λ_M 10^{-3}(Ω^{-1} cm^2 mol^{-1}) = 9.8. λ_{max} in DMF, 43,759, 28,326, 21,413 (ε = 1058 L M^{-1} cm^{-1}). μ_{eff} (BM): 1.87.

[CuL^2(CBDCA)] (**2**) Yield: (1.7 g, 58%.). m.pt: 180–185 °C. Anal. Calc. for $C_{30}H_{28}N_2O_4Cu$: Cu, 11.9; C, 66.2; H, 5.2; N, 5.1; Found: Cu, 11.8; C, 66.1; H, 5.1; N, 5.0 (%). IR (KBr pellet, cm^{-1}): 1681 ν(non-coordinated C=O in CBDCA); 1603 ν(C=N); 1503 ν(−HC=C); 1328 ν(−C–O); 513 ν(M–O); 430 ν(M–N). MS *m/z*: 545 (56.4%) $[M+1]^+$. $\Lambda_M 10^{-3}$ (Ω^{-1} cm^2 mol^{-1}) = 9.6. λ_{max} (cm^{-1}) in DMF, 40,362, 29,642, 21,786 (ε = 1102 L M^{-1} cm^{-1}). μ_{eff} (BM): 1.89.

[CuL^3(CBDCA)] (**3**) Yield: (1.6 g, 50%). m.pt: 180–187 °C. Anal. Calc. for $C_{30}H_{28}N_2O_6Cu$: Cu, 11.7; C, 62.6; H, 4.8; N, 4.9; Found: Cu, 11.6; C, 62.4; H, 4.7; N, 4.8 (%). IR (KBr pellet, cm^{-1}): 3434 ν(−OH); 1689 ν(non-coordinated C=O in CBDCA); 1609 ν(−C=N); 1529 ν(−HC=C); 1325 ν(−C–O); 529 ν(M–O); 433 ν(M–N). MS *m/z*: 577 (51.8%) $[M+1]^+$. Λ_M 10^{-3} (Ω^{-1} cm^2 mol^{-1}) = 11.3. λ_{max} (cm^{-1}) in DMF, 41,424, 29,302, 21,186 (ε = 1084 L M^{-1} cm^{-1}). μ_{eff} (BM): 1.86.

[CuL^4(CBDCA)] (**4**).Yield: (1.7 g, 51%). m.pt: 184–190 °C. Anal. Calc. for $C_{32}H_{32}N_2O_6Cu$: Cu, 10.5; C, 63.6; H, 5.3; N, 4.6; Found: Cu, 10.4; C, 63.5; H, 5.2; N, 4.5 (%). IR (KBr pellet, cm^{-1}): 1680 ν(non-coordinated C=O in CBDCA); 1607ν(−C=N); 1522 ν(−HC=C); 1313ν(−C–O); 1272, 1081,ν(−C–O–C–); 532 ν(M–O); 440 ν(M–N). MS *m/z*: 605 (57.3%) $[M+1]^+$. Λ_M 10^{-3} (Ω^{-1} cm^2 mol^{-1}) = 10.1. λ_{max} (cm^{-1}) in DMF, 41,549, 27,821, 21,598 (ε = 1113 L M^{-1} cm^{-1}). μ_{eff} (BM): 1.85.

[ZnL^1(CBDCA)] (**5**) Yield: (2.0 g, 59%). m.pt: 180–186 °C. Anal. Calc. for $C_{30}H_{26}N_4O_8Zn$: Zn, 10.3; C, 57.; H, 4.1; N, 8.8; Found: Zn, 10.2; C, 56.9; H, 4.0; N, 8.7 (%). IR (KBr pellet, cm^{-1}): 1677 ν(non-

Table 8
Effect of Cu(II) complexes on hematological parameters of EAC tumor bearing mice.

Design of treatment	Hb (g %)	RBC 10^6 Cells/CU.MM	WBC 10^3 Cells/CU.MM	Total protein mg%	PCV (%)	Differential count (%)		
						Lymphocytes	Neutrophils	Monocytes
Normal	12.92 ± 0.15	4.9 ± 0.12	6.78 ± 0.14	5.73 ± 0.26	16.86 ± 0.55	66.46 ± 1.36	32.6 ± 1.61	1.25 ± 0.45
Tumor control	5.78 ± 0.42[a]	2.46 ± 0.14[a]	18.74 ± 0.47[a]	12.23 ± 0.34[a]	25.98 ± 0.56[a]	26.23 ± 1.16[a]	72.8 ± 1.07[a]	1.20 ± 0.45
1	12.18 ± 0.21[d]	4.18 ± 0.19[d]	15.58 ± 0.27[a,d]	7.19 ± 0.17[b,d]	17.64 ± 0.24[d]	66.08 ± 0.86[d]	36.12 ± 1.24[d]	1.17 ± 0.32
2	11.34 ± 0.12[d]	3.42 ± 0.15[a,e]	14.95 ± 0.54[a,d]	7.63 ± 0.27[a,d]	16.98 ± 0.51[d]	64.63 ± 1.09[d]	31.60 ± 1.23[d]	0.94 ± 0.24
3	11.09 ± 0.16[a,d]	3.98 ± 0.17[b,d]	12.16 ± 0.63[a,d]	8.56 ± 0.11[a,d]	17.18 ± 0.45[d]	63.42 ± 1.28[d]	33.27 ± 1.06[d]	1.03 ± 0.15
4	13.12 ± 0.14[d]	4.14 ± 0.15[d]	15.67 ± 0.42[a,d]	9.96 ± 0.41[a,d]	19.98 ± 0.58[b,d]	65.84 ± 1.24[d]	38.71 ± 1.13[d]	1.06 ± 0.23

[a]P<0.001:;[b]P < 0.01; [c]P < 0.05 *versus* Normal.
[d]P < 0.001; [e]P < 0.01 *versus* Tumor control. Data were analyzed by using one way ANOVA followed by Tukey–Kramer multiple comp.

coordinated C=O in CBDCA); 1618 ν(−C=N); 1509 ν(−HC=C); 1461, 1304, 839 ν(−C−N str; $-NO_2$); 1312 ν(−C−O); 511 ν(M−O); 436 ν(M−N). ^{1}H NMR (ppm): (aromatic) 6.9–7.6 (m); (CH, 1H) 6.9 (q), CBDCA [(CH_2, J = 7.6, 2H) 3.2 (q), (CH_2, J = 14.8, 2H) 2.3 (q)],(−CH_3, 6H), 2.1 (s). ^{13}C NMR (ppm):176.5 (C_{13}), 170.6 (C_7), 153.1 (C_9), 146.8 (C_{12}), 136.8 (C_5), 134.3 (C_4), 127.6–129.2 (C_1 to C_3), 124.4 (C_{11}), 123.5 (C_{10}), 114.3 (C_6), 61.3 (C_{14}), 25.7 (C_{15}), 20.7 (C_8), (19.1) (C_{16}). MS m/z: 636 (62.4%) $[M+1]^+$. Λ_M 10^{-3} (Ω^{-1} cm^2 mol^{-1}) = 14.5. λ_{max} (cm^{-1}) in DMF, 42,257, 33,169. μ_{eff} (BM): diamagnetic.

[ZnL^2(CBDCA)] (**6**) Yield: (1.8 g, 61%). m.pt: 176–183 °C. Anal. Calc. for $C_{30}H_{28}N_2O_4Zn$: Zn, 11.9; C, 66.0; H, 5.8; N, 5.1; Found: Zn, 11.8; C, 65.9; H, 5.7; N, 5.0 (%). IR (KBr pellet, cm^{-1}): 1681 ν(non-coordinated C=O in CBDCA). 1607 ν(−C=N); 1523 ν(−HC=C); 1322 ν(−C−O); 519 ν(M−O), 448 ν(M−N). ^{1}H NMR (ppm): (aromatic) 6.9–7.4 (m); (CH, 1H) 6.9 (q), CBDCA [(CH_2, J = 7.1, 2H) 3.2 (q), (−CH_3, 6H), 2.2 (s), (CH_2, J = 14.2, 2H) 2.1 (q)]. ^{13}C NMR (ppm):176.4 (C_{13}), 170.1 (C_7), 136.8 (C_{16}), 136.7 (C_5), 136.2 (C_9), 134.4 (C_4), 130.3 (C_{11}), 127.8–129.2 (C_1 to C_3), 127.2 (C_{12}), 119.4 (C_{10}), 114.4 (C_6), 61.3 (C_{14}), 25.6 (C_{15}), 20.7 (C_8), (19.4) (C_{16}). MS m/z: 546 (65.2%) $[M+1]^+$. Λ_M 10^{-3} (Ω^{-1} cm^2 mol^{-1}) = 16.3. λ_{max} (cm^{-1}) in DMF, 40,762, 26,395. μ_{eff} (BM): diamagnetic.

[ZnL^3(CBDCA)] (**7**).Yield: (1.9 g, 60%). m.pt: 186–192 °C. Anal. Calc. for $C_{30}H_{28}N_2O_6Zn$: Zn, 11.3; C, 62.3; H, 4.9; N, 4.8; Found: Zn, 11.2; C, 62.2; H, 4.8; N, 4.7(%). IR (KBr pellet, cm^{-1}): 3433 ν(−OH); 1684 ν(non-coordinated C=O in CBDCA), 1611 ν(−C=N); 1526 ν(−HC=C); 1329 ν(−C−O); 519 ν(M−O), 431 ν(M−N). ^{1}H NMR (ppm):(C−OH, 1H) 10.4 (s), (CH, 1H) 6.9 (q), (aromatic) 6.8–7.4 (m); CBDCA [(CH_2, J = 7.4, 2H) 3.1(q), (CH_2, J = 14.8, 2H) 2.2 (q)],(−CH_3, 6H), 2.1 (s). ^{13}C NMR (ppm):175.9 (C_{13}), 170.2 (C_7), 157.2 (C_{12}), 145.2 (C_9), 136.7 (C_{16}), 136.5 (C_5), 133.7 (C_4), 127.6–129.4 (C_1 to C_3), 123.1 (C_{10}), 118.3 (C_{11}), 114.6 (C_6), 61.2 (C_{14}), 25.7 (C_{15}), 20.7 (C_8), (19.3) (C_{16}). MS m/z: 578 (56.8%) $[M+1]^+$. Λ_M 10^{-3} (Ω^{-1} cm^2 mol^{-1}) = 16.1. λ_{max} (cm^{-1}) in DMF, 41,550, 32,659. μ_{eff} (BM): diamagnetic.

[ZnL^4(CBDCA)] (**8**) Yield: (1.9 g, 58%) m.pt: 191–197 °C. Anal. Calc. for $C_{32}H_{32}N_2O_6Zn$: Zn, 10.7; C, 63.4; H, 5.3; N, 4.6; Found: Zn, 10.7; C, 63.3; H, 5.2; N, 4.5 (%). IR (KBr pellet, cm^{-1}): 1686 ν(non-coordinated C=O in CBDCA)0.1616 ν(−C=N); 1542 ν(−HC=C); 1324 ν(−C−O); 1261, 1085,ν(−C−O−C−); 526 ν(M−O), 435 ν(M−N). ^{1}H NMR (ppm): (aromatic) 6.9–7.6 (m); (CH, 1H) 6.9 (q), (−OCH_3, 3H) 3.9 (s), CBDCA [(CH_2, J = 7.5, 2H) 3.3 (q), (CH_2, J = 14.9, 2H) 2.3 (q)], (−CH_3, 6H), 2.3 (s). ^{13}C NMR (ppm):176.1 (C_{14}), 170.5 (C_7), 159.3 (C_{12}), 144.2 (C_9), 136.5 (C_5),133.6 (C_4), 127.8–129.5 (C_1 to C_3), 123.4 (C_{10}), 116.2 (C_{11}) 111.2 (C_6), 61.2 (C_{15}), 57.2 (C_{13}), 25.7 (C_{16}), 20.7 (C_8), 19.4 (C_{17}). MS m/z: 606 (67.4%) $[M+1]^+$. Λ_M 10^{-3} (Ω^{-1} cm^2 mol^{-1}) = 14.9. λ_{max} (cm^{-1}) in DMF, 42,451, 28,632. μ_{eff} (BM): diamagnetic.

6. Conclusion

In this research, the synthesis of complexes **1**–**8**, their structural characterization and *in vitro* strap interaction studies of novel mixed ligand complexes towards DNA and their cytotoxicity have been carried out. The results support the fact that the complexes effectively bind to DNA *via* intercalation. These intrinsic binding constant values are compared to cisplatin (standard drug) and ethidium bromide (classical intercalator) which reveals that K_b values of **1**–**8** are greater in magnitude than that of cisplatin ($5.73 \pm 0.45 \times 10^4$ M^{-1}), ethidium bromide (1.4×10^6 M^{-1}) and relatively lower than the metallointercalator $[Ru(bpy)_2(HBT)]^{2+}$ (5.71×10^7 M^{-1}). Fascinatingly, the complexes **1** and **5** follow the hydrolytic cleavage pathway (hydroxyl radical ($OH^{\bullet}$)). Moreover, the complexes **1**–**4** exhibit excellent cytotoxic bustle against HeLa, HEp-2, Hep G2 and MCF-7 cancer cell lines without significantly affecting the normal NIH 3T3 cells and the IC_{50} value of the complex **1** shows that the activity is higher than that of other complexes (**2**–**4**) and standard drugs. Particularly, admirable cytotoxic specificity against Hep G2 (human liver carcinoma cells) and the IC_{50} value of the complex **1** shows that the activity is about three times higher than that of cisplatin and two times higher than that of carboplatin. Further studies are needed to appraise its pharmacological properties *in vivo* and to elucidate the actual mechanism of its biological activity. These findings clearly indicate that the Cu(II) complexes may have potential with the biological target DNA, thereby affecting cellular responses akin to DNA strap interaction, damage and cytotoxic profile. Thus, the Cu(II) complexes are dominating over the others and proving their worth as robust and better choice for potent and safe chemotherapeutic drug design.

Acknowledgments

The authors express their heartfelt thanks to the Science & Engineering Research Board (SERB), DST (File No. SR/S1/IC-27/2012) New Delhi, India for financial support. They also express their gratitude to the College Managing Board, Principal and Head of the Department of Chemistry, VHNSN College, Virudhunagar for providing research facilities. They thank Prof. R. Senthil Kumar, Department of Pharmaceutical Chemistry, Swami Vivekanandha College of Pharmacy, Elayampalayam, Tiruchengodu, for *in vitro* and *in vivo* anti-cancer studies.

Appendix A. Supplementary data

Supplementary data related to this article can be found at http://dx.doi.org/10.1016/j.ejmech.2014.08.036.

References

[1] M.C. Prabhakara, B. Basavaraju, H.S. Bhojya Naik, Co(III) and Ni(II) complexes containing bioactive ligands: synthesis, DNA binding, and photocleavage studies, Bioinorg. Chem. Appl. 2007 (2007) 36497.
[2] R. Manikandan, P. Viswnathamurthi, Coordination behavior of ligand based on NNS and NNO donors with ruthenium(III) complexes and their catalytic and DNA interaction studies, Spectrochim. Acta A 97 (2012) 864–870.
[3] M.J. Hannon, Metal-based anticancer drugs: from a past anchored in platinum chemistry to a post-genomic future of diverse chemistry and biology, Pure Appl. Chem. 79 (2007) 2243–2261.
[4] T. Stringer, B. Therrien, D.T. Hendricks, H. Guzgay, G.S. Smith, Mono- and dinuclear (η6-arene) ruthenium(II) benzaldehyde thiosemicarbazone complexes: synthesis, characterization and cytotoxicity, Inorg. Chem. Commun. 14 (2011) 956–960.
[5] H. Liu, X. Shi, M. Xu, Z. Li, L. Huang, D. Bai, Z.Z. Zeng, Transition metal complexes of 2, 6-di ((phenazonyl-4-imino) methyl)-4-methylphenol: structure and biological evaluation, Eur. J. Med. Chem. 46 (2011) 1638–1647.
[6] F. Arjmand, A. Jamsheera, D.K. Mohapatra, Synthesis, characterization and in vitro DNA binding and cleavage studies of Cu(II)/Zn(II) dipeptide complexes, J. Photochem. Photobiol. B Biol. 121 (2013) 75–85.
[7] E. Ramachandran, D.S. Raja, N.S.P. Bhuvanesh, K. Natarajan, Synthesis, characterization and in vitro pharmacological evaluation of new water soluble Ni(II) complexes of 4N-substituted thiosemicarbazones of 2-oxo-1,2-dihydroquinoline-3-carbaldehyde, Eur. J. Med. Chem. 64 (2013) 179–189.
[8] Z.C. Liu, B.D. Wang, Z.Y. Yang, Y. Li, D.D. Qin, T.R. Li, Synthesis, crystal structure, DNA interaction and antioxidant activities of two novel water-soluble Cu(2+) complexes derivated from 2-oxo-quinoline-3-carbaldehyde Schiff-bases, Eur. J. Med. Chem. 44 (2009) 4477–4484.
[9] J.X. Chen, W.E. Lin, C.Q. Zhou, L.F. Yau, J.R. Wang, B. Wang, W.H. Chen, Z.H. Jiang, Synthesis, crystal structures and biological evaluation of water-soluble zinc complexes of zwitterionic carboxylates, Inorg. Chim. Acta 376 (2011) 389–395.
[10] B. Zhao, X.Y. Cheng, Design and synthesis of 3d–4f metal-based zeolite-type materials with a 3D nanotubular structure encapsulated "Water" pipe, J. Am. Chem. Soc. 126 (2004) 3012–3013.
[11] X.L. Wang, C. Qin, E.B. Wang, Y.G. Li, C.W. Hu, L. Xu, $[Cu_2(HBTC)_2(H_2O)_2$ (μ2-$H_2O)]\cdot 2H_2O$: N new arm-shaped two-dimensional copper coordination polymer having both rhombic cavities and helical-like channels, Inorg. Chem. Commun. 7 (2004) 788–791.
[12] S. Schreier, S.V.P. Malheiros, E. de Paula, Surface active drugs: self-association and interaction with membranes and surfactants. Physicochemical and biological aspects, Biochim. Biophys. Acta Biomembr. 1508 (2000) 210–234.

[13] S. Shujha, A. Shah, Z. Rehman, N. Muhammad, S. Ali, R. Qureshi, N. Khalid, A. Meetsma, Diorganotin(IV) derivatives of ONO tridentate Schiff base: synthesis, crystal structure, in vitro antimicrobial, anti-leishmanial and DNA binding studies, Eur. J. Med. Chem. 45 (2010) 2902–2911.
[14] J.E. Weder, T.W. Hambley, B.J. Kennedy, P.A. Lay, G.J. Foran, A.M. Rich, Determination of the structures of antiinflammatory copper(II) dimers of indomethacin by multiple-scattering analyses of X-ray absorption fine structure data, Inorg. Chem. 40 (2001) 1295–1302.
[15] Q. Zhou, T.W. Hambley, B.J. Kennedy, P.A. Lay, P. Turner, B. Warwick, J.R. Biffin, H.L. Regtop, Syntheses and characterization of anti-inflammatory dinuclear and mononuclear zinc indomethacin complexes. Crystal structures of $[Zn_2(indomethacin)_4(L)_2]$ (L = N,N-dimethylacetamide), pyridine,1-methyl-2-pyrrolidinone) and $[Zn(indomethacin)_2(L1)_2]$ (L1 = ethanol, methanol), Inorg. Chem. 39 (2000) 3742–3748.
[16] D.D. Li, J.L. Tian, W. Gu, X. Liu, H.H. Zeng, S.P. Yan, DNA binding, oxidative DNA cleavage, cytotoxicity, and apoptosis-inducing activity of copper(II) complexes with 1,4-tpbd (N, N,N′,N′-tetrakis(2-yridylmethyl)benzene-1,4-diamine) ligand, J. Inorg. Biochem. 105 (2011) 894–901.
[17] R. Buchtik, Z. Travnicek, J. Vanco, In vitro cytotoxicity, DNA cleavage and SOD-mimic activity of copper(II) mixed-ligand quinolinonato complexes, J. Inorg. Biochem. 116 (2012) 163–171.
[18] C. Gokçe, R. Gup, Synthesis, characterization and DNA interaction of new copper(II) complexes of Schiff base-aroylhydrazones bearing naphthalene ring, J. Photochem. Photobiol. B Biol. 122 (2013) 15–23.
[19] N. Raman, S. Sobha, M. Selvaganapathy, Probing the DNA-binding behavior of tryptophan incorporating mixed-ligand complexes, Monatsh. Chem. 143 (2012) 1487–1495.
[20] M. Selvaganapathy, N. Raman, Chelating behavior and biocidal efficiency of tryptophan based mixed-ligand complexes, Inorg. Chem. Commun. 20 (2012) 238–242.
[21] N. Raman, N. Pravin, DNA fastening and ripping actions of novel Knoevenagel condensed dicarboxylic acid complexes in antitumor journey, Eur. J. Med. Chem. 80 (2014) 57–70.
[22] N. Raman, N. Pravin, Lasing the DNA fragments through β-diketimine framed Knoevenagel condensed Cu(II) and Zn(II) complexes – an in vitro and in vivo approach, Spectrochim. Acta A 118 (2014) 867.
[23] K. Nakamoto, Infrared and Raman Spectra of Inorganic and Coordination Compounds, fourth ed., Wiley, New York, 1986.
[24] W.G. Geary, The use of conductivity measurements in organic solvents for the characterisation of coordination compounds, Coord. Chem. Rev. 7 (1971) 81–122.
[25] A.B.P. Lever, Inorganic Electronic Spectroscopy, Elsevier, Amsterdam, 1984.
[26] A.W. Addison, Is ligand topology an influence on the redox potentials of copper complexes? Inorg. Chim. Acta 162 (1989) 217–220.
[27] R.K. Ray, G.B. Kauffman, EPR spectra and covalency of bis(amidinourea/o-alkyl-1-amidinourea)copper(II) complexes Part II. Properties of the CuN_4^{2-} chromophore, Inorg. Chim. Acta 173 (1990) 207–214.
[28] D.X. West, 2-aminopyridine N-oxide complexes formed from various copper(II) salts, Inorg. Nucl. Chem. 43 (1984) 3169–3174.
[29] H. Chao, W. Mei, Q. Huang, L. Ji, DNA binding studies of ruthenium(II) complexes containing asymmetric tridentate ligands, J. Inorg. Biochem. 92 (2002) 165–170.
[30] F.R. Keene, J.A. Smith, J.G. Collins, Metal complexes as structure-selective binding agents for nucleic acids, Coord. Chem. Rev. 253 (2009) 2021–2035.
[31] A.M. Pyle, T. Morri, J.K. Barton, Probing microstructures in double-helical DNA with chiral metal complexes: recognition of changes in base-pair propeller twisting in solution, J. Am. Chem. Soc. 112 (1990) 9432–9434.
[32] E.K. Efthimiadou, A. Karaliota, G. Psomas, Metal complexes of the third-generation quinolone antimicrobial drug sparfloxacin: structure and biological evaluation, J. Inorg. Biochem. 104 (2010) 455–466.
[33] C.N. N'soukpoe Kossi, C. Descoteaux, E. Asselin, H.A.T. Riahi, G. Berube, DNA interaction with novel antitumor estradiol–platinum(II) hybrid molecule: a comparative study with cisplatin drug, DNA Cell. Biol. 27 (2008) 101–107.
[34] M.J. Waring, Complex formation between ethidium bromide and nucleic acids, J. Mol. Biol. 13 (1965) 269–282.
[35] D.L. Arockiasamy, S. Radhika, R. Parthasarathi, B.U. Nair, Synthesis and DNA-binding studies of two ruthenium(II) complexes of an intercalating ligand, Eur. J. Med. Chem. 44 (2009) 2044–2051.
[36] Y.J. Liu, X.Y. Wei, W.J. Mei, L.X. He, Synthesis, characterization and DNA binding studies of ruthenium(II) complexes: $[Ru(bpy)_2(dtmi)]^{2+}$ and [Ru(bpy)2(dtni)]$^{2+}$, Trans. Met. Chem. 32 (2007) 762–768.
[37] S.B. Satish, A.K. Anupa, H. Hussain, A.K. Ayesha, V.G. Vivekanand, P.G. Shridhar, G.P. Vedavati, Synthesis, electronic structure, DNA and protein binding, DNA cleavage, and anticancer activity of fluorophore-labeled copper(II) complexes, Inorg. Chem. 50 (2011) 545–558.
[38] U. Chaveerach, A. Meenongwa, Y. Trongpanich, C. Soikum, P. Chaveerach, DNA binding and cleavage behaviors of copper(II) complexes with amidino-*o*-methylurea and N-methylphenyl-amidino-*o*-methylurea, and their antibacterial activities, Polyhedron 29 (2010) 731–738.
[39] S. Mahadevan, M. Palaniandavar, Spectroscopic and voltammetric studies on copper complexes of 2,9-dimethyl-1,10-phenanthrolines bound to calf thymus DNA, Inorg. Chem. 37 (1998) 693–700.
[40] A.W. Wallace, W.R. Murphy, J.D. Petersen, Electrochemical and photophysical properties of mono- and bimetallic ruthenium(II) complexes, Inorg. Chim. Acta 166 (1989) 47–54.
[41] R. Ramesh, S. Maheswaran, Synthesis, spectra, dioxygen affinity and antifungal activity of Ru(III) Schiff base complexes, J. Inorg. Biochem. 96 (2003) 457–462.
[42] Y. Anjaneyulu, R.P. Rao, Characterization and antimicrobial activity studies on some ternary complexes of Cu(II) with acetylacetone and various salicylic acids, Synth. React. Inorg. Org. Chem 16 (1986) 257–272.
[43] A.Z. El-Sonbati, M.A. Diab, A.A. El-Bindary, S.G. Nozha, Structural and characterization of novel copper(II) azodye complexes, Spectrochim. Acta A 83 (2011) 490–498.
[44] C. Oberling, M. Guerin, The role of viruses in the production of cancer, Adv. Cancer Res. 2 (1954) 353–423.
[45] H.C. Hogland, Heamatological complications of Cancer chemotherapy, Semin. Oncol. 9 (1982) 95–102.
[46] P.E. Price, R.E. Greenfield, J.P. Greenstein, A. Haddow (Eds.), Advances in Cancer Research, Academic Press, New York, 1950, pp. 199–200.
[47] M. Maseki, I. Nishiagaki, M. Hagishara, Y. Tamoda, K. Yagi, Lipid peroxidation levels and lipid content of serum lipoprotein fractions of pregnant subjects with or without preeclamsia, Clin. Chim. Acta 41 (1981) 424–426.
[48] L.D. Fenninger, L.D. Mider, G.B. In, J.P. Greenstein, A. Haddow (Eds.), Advances in cancer Research, Academic Press, New York, 1954, pp. 244–250.